EEET ECOLOGICAL ENGINEERING & ENVIRONMENTAL TECHNOLOGY

Ecological Engineering & Environmental Technology 2024, 25(6), 172–187
https://doi.org/10.12912/27197050/186922
ISSN 2719-7050, License CC-BY 4.0

Received: 2024.03.09
Accepted: 2024.04.22
Published: 2024.05.01

Simultaneous Adsorption of Rare Earth Metal Ions on Chitosan-Coated Fumed Silica – Characterization, Kinetics, and Isotherm Studies

Nurul Amirah Abd Aziz[1], Zul Adlan Mohd Hir[1], Wan Khaima Azira Wan Mat Khalir[2], Waheeba Ahmed Al-Amrani[3], Megat Ahmad Kamal Megat Hanafiah[1*]

[1] Department of Chemistry, Universiti Teknologi MARA, Cawangan Pahang, 26400, Jengka, Pahang, Malaysia
[2] Malaysia-Japan International Institute of Technology, Universiti Teknologi Malaysia, Jalan Sultan Yahya Petra, 54100 Kuala Lumpur, Malaysia
[3] Department of Chemistry, College of Science, Ibb University, Ibb, Yemen
* Corresponding author's e-mail: makmh@uitm.edu.my

ABSTRACT

The present study manufactured and utilized the chitosan-coated fumed silica composite (CS@silica) for simultaneous adsorption of rare earth elements (REEs) of Ce(III), La(III), and Nd(III) cations in an aqueous solution. The CS@silica composite underwent characterization using a CHNOS analyzer, Brunauer-Emmett-Teller (BET) surface area analyzer, attenuated total reflectance Fourier transform infrared (ATR-FTIR) spectrophotometer, scanning electron microscope coupled with energy-dispersive X-ray (SEM-EDX) spectrophotometer, and X-ray diffraction (XRD) analyzer. The findings indicated that the CS@silica composite exhibited a lack of pores and possessed a specific surface area of 1.27 m^2/g. Additionally, it was observed that the composite contained a significant amount of oxygen and nitrogen atoms, which serve as the active sites for the adsorption of REEs. The maximum adsorption capacities of Ce(III), La(III), and Nd(III) cations were determined under optimal experimental conditions. These parameters included a pH of 4, an adsorbent dose of 0.01 g, and an equilibrium duration of 20 min. The maximum adsorption capacities for Ce(III), La(III), and Nd(III) cations were found to be 341, 241, and 299 mg/g, respectively. The adsorption kinetics followed the pseudo-second-order kinetic model. The desorption percentage of REEs-loaded CS@silica composite was significantly low when exposed to deionized water and hydrochloric acid (0.01 and 0.02 M). This suggests that there is a chemical interaction between the REEs and the active site on the surface of the composite. The predominant adsorption process proposed was complexation, with ion exchange and electrostatic contact playing a minor role. The CS@silica composite is highly promising for the recovery of REEs because of its rapid adsorption and high adsorption capacities.

Keywords: adsorption, chitosan, fumed silica, isotherm, kinetics, rare-earth elements.

INTRODUCTION

Rare earth elements (REEs) are "seeds of technology" due to the demand for innovative or advanced materials. High-purity REEs are used in automotive catalytic converters, cathode ray tubes, permanent magnets in sound and computer systems, phosphors, lasers, smartphones, optical fibers, electric motors, and conceivable upcoming applications like colored pigments for plastics and paints, refrigeration systems, solid oxide fuel cells, and new catalysts due to their exceptional physical, chemical, catalytic optical, magnetic, and metallurgical (Sastri et al., 2003; Ponou et al., 2014). Various countries such as Switzerland, China, and Austria use REEs in aquaculture, zootechnics, and agriculture as growth enhancers in fish and crop production. New REE uses in nuclear medicine and fluorescence technology are being developed (Arciszewska et al., 2022).

REEs are abundant in the earth's crust, but depletion of high-grade ores and high mining

costs make them uncommon. Recent trade limitations on REE shipments from China have caused a global supply crisis, prompting the US and EU to classify REEs as vital resources (Ryu et al., 2021). Thus, sustainable separation and recovery from industrial and urban wastes is needed to replace main production and build a circular budget for REEs.

Different researchers found that mining effluent includes high heavy metal and REE concentrations (Iftekhar et al., 2022). Ecosystems are threatened by bioaccumulation of these nondegradable materials. High REE exposure is connected to lung and pancreatic malignancies, anorexia, stomach distension, indigestion, diarrhea, and fatigue. REEs can also limit plant growth and cause acute soil toxicity, genotoxicity and neurotoxicity in animals, human neurological disease, trophic bioaccumulation, carcinogenicity, and male sterility. Children are more at risk because radioactive waste generated from REE mining and processing activities can impair IQ and cause memory loss (Arciszewska et al., 2022). Additionally, the trivalent La(III) ionic radius is identical to the Ca(II) ion. Proteins and tissues' biological roles for Ca(II) ion can be duplicated and replaced by La(III). Numerous REEs have also been demonstrated to cause oxidative stress and DNA structural changes, which can cause cancer (Martinez-Gomez et al., 2016; Qiu et al., 2022; Jemli et al., 2023). So, REEs must be recovered from secondary sources like liquid effluents or leachates.

Adsorption is a potential approach for collecting REEs due to its simplicity, cheap operational cost, low energy consumption, reusability, and great effectiveness in selectively recuperating low REE concentrations (Asadollahzadeh et al., 2021). For REE adsorption from an aqueous solution, a preferred adsorbent must be abundant, low-cost, easy to fabricate, and have high adsorption capacity. Silica has fast adsorption, robust thermal (up to 1500 °C) and chemical stability, stiffness, selectivity, ion exchange probable, abundance, and swelling/shrinking resistance (Al-Amrani et al., 2022). However, silica particles have a low adsorption capability, notably for REEs (Ryu et al., 2021). This constraint can be overcome by careful modification of silica with functional material to create new composites that combine their good qualities and rearrange them to perform better than their individual components.

Linear polysaccharide chitosan (CS) from crustacea exoskeletons enriched hydrophilicity functional groups of OH and metal chelation through NH_2 groups made it effective in adsorption (Ahmed et al., 2020; Zhao et al., 2020). Though, thermal resistance, acid solubility, low surface area, weak mechanical performance, and low reusability limit its use (Liu et al., 2021; Benettayeb et al., 2023). Therefore, silica and CS may produce composites with better characteristics and satisfactory REE recovery from aqueous solutions. This coupling strategy is interesting since such composites are likely to improve structure heterogeneity, functionality, thermal stability, porosity, surface area, adsorption capacity, and dispersibility in aqueous solution. Laki´c et al. (2023) found that hybrid silica-based nano-adsorbents had faster adsorption of Ni(II) and Co(II) ions and better affinity for REEs of Sm(III) and Nd(III) ions. At an equilibrium duration of 6 h, Ni(II) and Co(II) ions adsorb 1.45 and 1.18 mmol/g, respectively, followed by Sm (0.56 mmol/g) and Nd (0.47 mmol/g). According to Ryu et al. (2021), virgin SBA-15 silica had low adsorption ability for REEs of Lu and Y, while 1,4-Phthaloyl diamido-propyltriethoxysilane ligand-modified Santa Barbara Amorphous silica-15 (1,4-PA-SBA-15) silica recovered 17.9 and 17.0 mg/L, respectively. Salih et al. (2021) found that mesoporous amine-functionalized polymer/silica composite adsorbs REEs of Gd(III) and Nd(III) cations at pH 4 and equilibrium duration of 30–40 min with maximum capacities of 1.0 and 0.9 mmol/g, respectively. The adsorbent demonstrated remarkable selectivity for REEs over alkali-earth elements Ca(II), Mg(II), and Sc(III) at pH 4–5. 4-*tert*-Octyl-4-((phenyl)diazenyl)phenol (TOPP) anchoring onto silica matrix separated and recovered Yb(III) ions by Rahman et al. (2020). The greatest Yb(III) adsorption was 139.19 mg/g at 60 min and pH 5. The bond distance between Yb-O and Yb-N was 2.206 and 2.847 Å, indicating that the O-atom donated less than the N-atom in the produced organic ligand. Though, both atoms coordinated with Yb(III) ions to form stable complexation and coordination (Rahman et al., 2020). Another study reported that DTPA-CS–silica had a greater adsorption capacity and selectivity for Nd(III) ions than EDTA-CS–silica (Roosen et al., 2014). Although these studies demonstrate different levels of enhancement in the recovery of REEs, additional research is required to address operational difficulties and enhance the recyclability of adsorbents.

In this study, we suggest utilizing CS@silica to test the retrieval of Ce(III), La(III), and Nd(III)

ions simultaneously from aqueous solutions under batch mode. Chitosan, when combined with inorganic adsorbents such as fumed silica, creates adsorbent materials that have rapid adsorption kinetics, increased pH tolerance, and a high capacity (Budnyak et al., 2020). However, there have yet to be any published papers on the utilization of CS@silica for the simultaneous adsorption of REEs from aqueous solutions. The influence of CS@silica's physicochemical features on the adsorption of the examined REEs was thoroughly examined. Initially, a thorough analysis of the physicochemical properties of CS, fumed silica (FS), and CS@silica was conducted, which involved various methods such as BET surface area, SEM-EDX, ATR-FTIR, XRD, and pH of point of zero charge (pH_{pzc}). In addition, the performance of CS@silica for REE adsorption was assessed based on the influence of pH, adsorption time, adsorbent dose, kinetics, and isotherms.

MATERIALS AND METHODS

Materials and chemicals

CS powder (85% degree of deacetylation which provides a high concentration of amino groups), fumed silica (SiO_2, 99%), CH_3COOH (≥ 99.5%), NaOH pellets, HCl (37%), NaCl, ionic liquid; 1-ethyl-3-methyl-imidazolium acetate ($C_8H_{14}N_2O_2$, 97%) and epichlorohydrin (C_3H_5ClO, 99%) were purchased from Aldrich. $Ce(NO_3)_3 \cdot 6H_2O$ (99.5%, Merck), $Nd(NO_3)_3 \cdot 6H_2O$ (99.9%, Merck), $La(NO_3)_3 \cdot 6H_2O$ (99.9%, Merck). All the reagents used were of analytical grade.

Preparation of REE solutions

A standard solution containing 1000 mg/L of each REE was made, and the necessary concentrations were achieved by diluting it with deionized water. The concentration of Ce(III), La(III), and Nd(III) ions before and after the adsorption process was analyzed using an Inductively Coupled Plasma-Optical Emission Spectrophotometer (ICP-OES, Agilent 5110, USA).

Preparation of CS@silica

CS@silica was prepared as follows: two grams of CS powder were added to a mixture containing 2 mL of ionic liquid, 3 mL (2% v/v) acetic acid, and 100 mL of distilled water and stirred for 10 min using a magnetic stirrer until complete dissolution of CS particles. After that, 9.0 g of FS was added to the mixture and continuously stirred for 24 h at room temperature. Then, the mixture was dropped using a micropipette into 500 mL of 0.50 M NaOH solution and left for 15 min, followed by adding 125 mL of 0.10 M epichlorohydrin to the mixture and left again for 2 h. The CS@silica formed was filtered and washed with distilled water before being dehydrated in an oven for 24 h at 40 °C, ground, separated to a particle size of 250 nm, and stored in a container for further usage. Figure 1 depicts the synthetic pathway for the CS@silica composite.

Characterization of CS@silica

The elemental analysis of CS, FS, and CS@silica was measured using a CHNSO analyzer (PerkinElmer, 2400 Series II, USA). The BET analysis of CS, FS, and CS@silica was measured using a surface area analyzer (Micrometrics ASAP 2010, USA). The analysis commenced by degassing the adsorbents at 90 °C for 2 h to eliminate any physically adsorbed gas. The N_2 adsorption-desorption curves were plotted as well, and the specific surface area values were considered from the BET (S_{BET}) and Langmuir (S_L) isotherm plots. The pH_{pzc} was performed in a series of 50 mL of 0.01 M NaCl solutions prepared using Erlenmeyer flasks. The pH of the solution was attuned from 2 to 9 by the addition of 1.0 M of HCl and NaOH solutions into a series of Erlenmeyer flasks. Then, 0.10 g of CS@silica was added to each flask. The mixture was agitated using a magnetic stirrer for 1 h at room temperature. Then, the CS@silica was filtered and dried overnight at room temperature. The X-ray diffraction (XRD) analysis was conducted using an X-ray diffractometer (Malvern Panalytical X'pert PRO, Netherlands) at 45 kV and a current of 30 mA with Cu-K_α radiation. The XRD pattern was initiated to scan from 10 to 80° at a 2θ angle. Functional groups in CS, FS, and CS@silica were identified using the attenuated total reflectance Fourier transform infrared (ATR-FTIR) spectrophotometer (PerkinElmer, Spectrum 100, USA). A scanning electron microscope coupled with energy dispersive X-ray (SEM-EDX, TESCAN, Czech Republic) was used to examine the external structure and

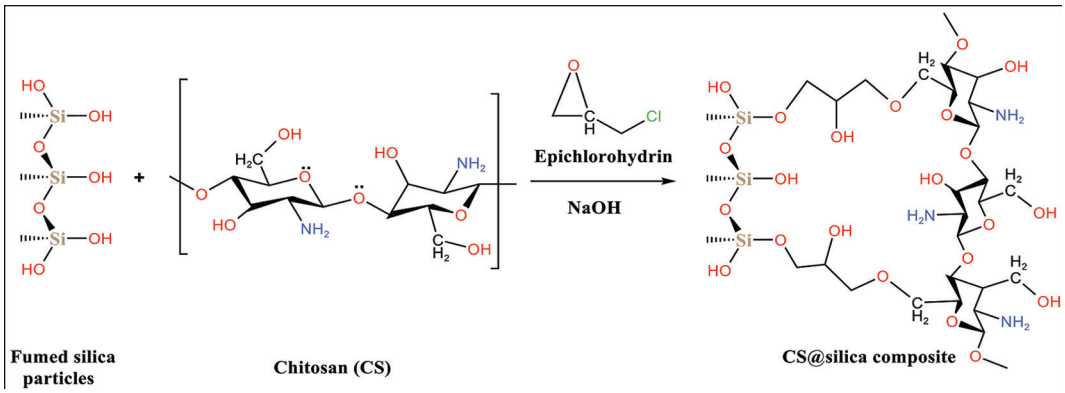

Figure 1. Synthesis route of CS@silica composite

elemental configuration of CS, FS, and CS@silica before and after REEs adsorption.

REEs adsorption tests

The tests for adsorption of REEs were conducted concurrently in aqueous solutions using a batch technique. The tests were replicated, and the reported results signify the mean findings. In the experiment, a composite of CS@silica weighing 0.01g and a mixture of Ce(III), Nd(III), and La(III) with concentrations of 0.20 mmol/L (equivalent to 28.02, 28.85, and 27.78 mg/L respectively) were employed, unless specified otherwise. An experiment was undertaken to analyze the influence of pH within a range of 2 to 6. The pH levels were modified by utilizing a 1 mol/L solution of HCl and NaOH and agitated for 1 h using a magnetic stirrer. The impact of the CS@silica dose was investigated by utilizing varying amounts of 0.010, 0.015, 0.020, and 0.025 g and stirring the mixture for 1 h. After undergoing filtration, the concentrations of Ce(III), Nd(III), and La(III) ions were measured by ICP-OES. The quantity of REEs adsorbed (q_t, mg/g) on CS@silica and the removal percentage were determined using the following equations:

$$q_t = \frac{(C_o - C_t)V}{m} \quad (1)$$

$$Removal\ (\%) = \frac{(C_o - C_t)}{C_o} \times 100 \quad (2)$$

where: C_o and C_t are REE concentrations before and after adsorption (mg/L or mmol/g), respectively; V is the volume of REE solution (L), and m is the weight of CS@silica (g).

Desorption study

This study was carried out to examine the adsorption and desorption characteristics of 0.01 g of CS@silica in 50 mL (0.40 mmol/L) of aqueous solutions containing Ce(III), Nd(III), and La(III) cations. The solution was vigorously stirred for 1 h before being subjected to filtration, and the resultant liquid was analyzed using ICP-OES. The REEs-loaded CS@silica was subjected to drying at a temperature of 80 °C for 2 h. Subsequently, the sample underwent a desorption experiment with deionized water and HCl solutions with concentrations of 0.01 and 0.02 mol/L, respectively. The contents were vigorously stirred for 1 h before undergoing filtration and subsequent analysis with ICP-OES. The desorption percentage was calculated using the following equation:

$$D_p\ (\%) = \frac{C_{des}}{C_{ads}} \times 100 \quad (3)$$

where: C_{des} and C_{ads} are REEs concentration desorbed and adsorbed, respectively.

Adsorption kinetic and isotherm

The REEs adsorption kinetic experiment was carried out at two initial concentrations of 0.20 and 0.40 mmol/L at optimal conditions of 0.01 g of CS@silica dosage and pH 4. The mixture was agitated for 1 to 60 min at room temperature (30 ± 0.5 °C), filtered, and analyzed using ICP-OES. Traditional non-linear pseudo-first-order (PFO, Eq. 4) (Lagergren, 1898) and pseudo-second-order (PSO, Eq. 5) (Ho and McKay, 1999) were performed in the kinetic adsorption modeling.

$$q_t = q_e\ (1 - e^{-k_1 t}) \quad (4)$$

$$q_t = \frac{qe^2\ k_2 t}{q_e k_2 t + 1} \quad (5)$$

where: q_e and q_t are the quantity of REEs adsorbed per weight of CS@Silica (mg/g) at steadiness and at any time t (min), respectively; k_1 (1/min) and k_2 (g/mg.min) are rate constants of the PFO and PSO kinetic models, respectively. The adsorption isotherm experiments of REEs were set at room temperature and best settings of pH 4, adsorbent dose of 0.01 g and steadiness time of 60 min. The concentrations of REEs used were in the range of 0.20 to 1.20 mmol/L.

Statistical analysis

In order to align the investigative findings more accurately with the desired models, a non-linear regression evaluation of the isotherm and kinetic models was conducted by means of the Solver add-in for Microsoft Excel. The assessment of the fitness level was carried out using statistical methods, specifically the determination constant (R^2) and the non-linear chi-square ($\chi 2$). The statistical properties were computed using the following mathematical equations:

$$R^2 = \frac{\Sigma(q_{e,cal,i} - q_{e,exp,i})^2}{\Sigma(q_{e,cal,i} - q_{e,exp,avg})^2 - \Sigma(q_{e,cal.i} - q_{e,exp,i})^2} \quad (6)$$

$$\chi^2 = \sum_{i=1}^{N} \left| \frac{(q_{e,exp,i} - q_{e,cal,i})^2}{q_{e,exp,i}} \right| \quad (7)$$

RESULTS AND DISCUSSION

Characterization studies

Table 1 presents the elemental composition analysis of CS, FS, and CS@silica. The contents of C, H, and N atoms on the FS surface show a substantial rise of 21.03, 5.72, and 4.03%, respectively, after being coated with CS particles. The concentration of oxygen atoms reduced from 99.17 to 69.03% on the CS@silica surface, indicating the interaction of silanol groups with the crosslinker (refer to Figure 1). These modifications validate the effective application of the coating on the FS surface by utilizing the amine and hydroxyl groups of CS particles and the silanol groups of the FS surface (Budnyak et al., 2020). The coating of FS particles with CS material was confirmed by the significant reduction in the surface area of the raw FS particles (S_{BET} and S_L) from 343.37 and 2050.29 to 1.27 and 13.34 m^2/g for CS@silica composite, respectively. This suggests that the crosslinker and chitosan molecules blocked the pores in FS after the coating process. Furthermore, the significant upsurge in the average pore width from 108.98 Å (FS particle) to 343.23 Å (CS@silica) provides confirmation of the presence of the crosslinker and CS as thin layers on the FS surface (refer to Figure 1). Previous studies in the literature have reported similar findings (Roosen et al., 2014; Budnyak et al., 2020; Ryu et al., 2021).

The pH_{pzc} results of the CS@silica composite are shown in Figure 2. The graph illustrates that the CS@silica surface exhibits acidic properties with negative pH values at low pH levels. As the pH increases, the surface gradually becomes less negative pH values until it approaches a neutral charge at a pH of 8.47. This pH value is known as the point of zero charge (pH_{pzc}). It also indicates that the amount of positively charged functional groups is equal to the amount of negatively charged functional groups.

Figure 3(a-c) confirms the amorphous shape of the pristine FS and CS and the CS@silica composite through the XRD patterns. The large diffraction peak that emerges at 22.1° in the FS pattern was attributed to the characteristic amorphous form of silica nanoparticles. Chitosan was found to have a

Table 1. Elemental analysis for CS, FS, and CS@silica

Analysis	CS	FS	CS@silica
Carbon (%)	36.53±0.07	0.24±0.02	21.03±0.25
Oxygen (%)	48.87±0.05	99.17±0.18	69.03±0.39
Hydrogen (%)	7.61±0.03	0.45±0.06	5.72±0.17
Nitrogen (%)	6.94±0.00	0.09±0.00	4.03±0.04
S_{BET}[a] (m^2/g)	0.15	343.37	1.27
S_L[b] (m^2/g)	0.41	2050.29	13.43
D_p[c] (Å)	858.04	108.98	346.23

Note: [a]BET surface area, [b]Langmuir surface area, [c]Average pore diameter (BJH).

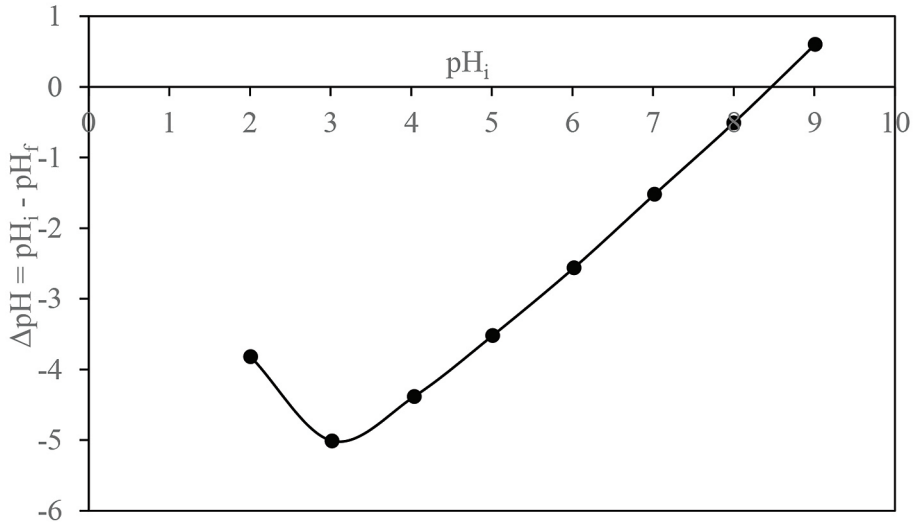

Figure 2. The pH_{pzc} plot of CS@silica composite

peak at 19.9°, which was somewhat more intense than FS. Both peaks of FS particles (Figure 3a) and CS (Figure 3b) showed up in the CS@silica pattern (Figure 3c), approving the effective coating of CS onto the FS surface. The outcomes are in agreement with those reported in preceding investigations (Atia et al., 2009; Feng et al., 2021).

The Fourier transform infrared spectroscopy (FTIR) spectra of CS, FS, CS@silica, and REEs-loaded CS@silica are presented in Figure 4. Figure 4a displays two separate peaks at 1078 and 808 cm^{-1}, representing the vibrations of υ(Si-O-Si) in the siloxane backbone, υ(Si-OH) in the free silanol group, and tetrahedron υ(SiO_4), respectively (Donia et al., 2009; Salih et al., 2021). However, many new characteristic bands appeared on FS after coating with CS molecules, as shown in Figure 4c**,** confirming the successful coating of FS particles with CS molecules. A broad band was observed at 3362 cm^{-1}, indicating the stretching of N-H and O-H groups. The N-H bending vibration in CS can be detected at 1589 cm^{-1}. Peaks at 2872 cm^{-1} and 1640 cm^{-1} correspond to C-H stretching vibrations of aliphatic groups and the presence of a carbonyl group, respectively, originating mainly from CS, as shown in Figure 4b. Around 1150–1028 cm^{-1}, peaks correspond to C-O and C-C stretching vibrations in the chitosan backbone

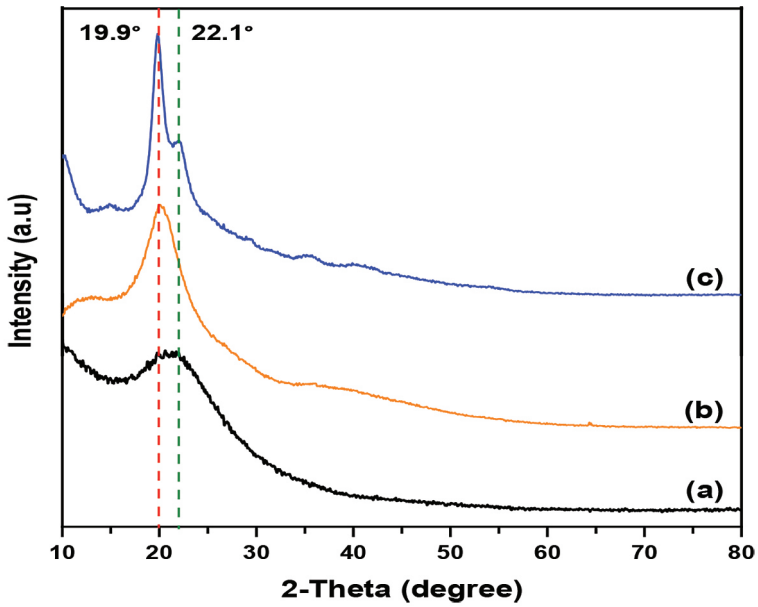

Figure 3. XRD forms of raw FS (a), CS (b) and CS@silica composite (c)

(Feng et al., 2021). The peak at 894 cm^{-1} is related to the glycosidic linkage between N-acetylglucosamine and glucosamine units (Budnyak et al., 2020). This suggests that the surface of the CS@silica composite contains a significant amount of –OH, $–NH_2$, and carbonyl bonds. Figure 4d shows similar peaks to the CS@silica composite (Figure 4c), except new characteristic peaks of 1491, 1452, 662, 695, and 755 cm^{-1} appeared, indicating the presence of the adsorbed REEs onto the CS@silica surface. Moreover, it was found that the vibration of a carbonyl group on CS@silica composite at 1640 cm^{-1} completely vanished after REEs adsorption because of its participation in the REEs adsorption. Furthermore, the diminished intensity of the wide peak at 3371 cm^{-1}, which resembles the vibrations of $–NH_2$ and –OH groups, can be observed in Figure 4d when compared to the CS@silica composite, confirming the binding of the REEs onto the CS@silica composite. Figure 5 shows the functional groups that are likely involved in the interaction with REEs that cause REEs to chelate or complex with CS molecules. Figure 6 shows the external structure of

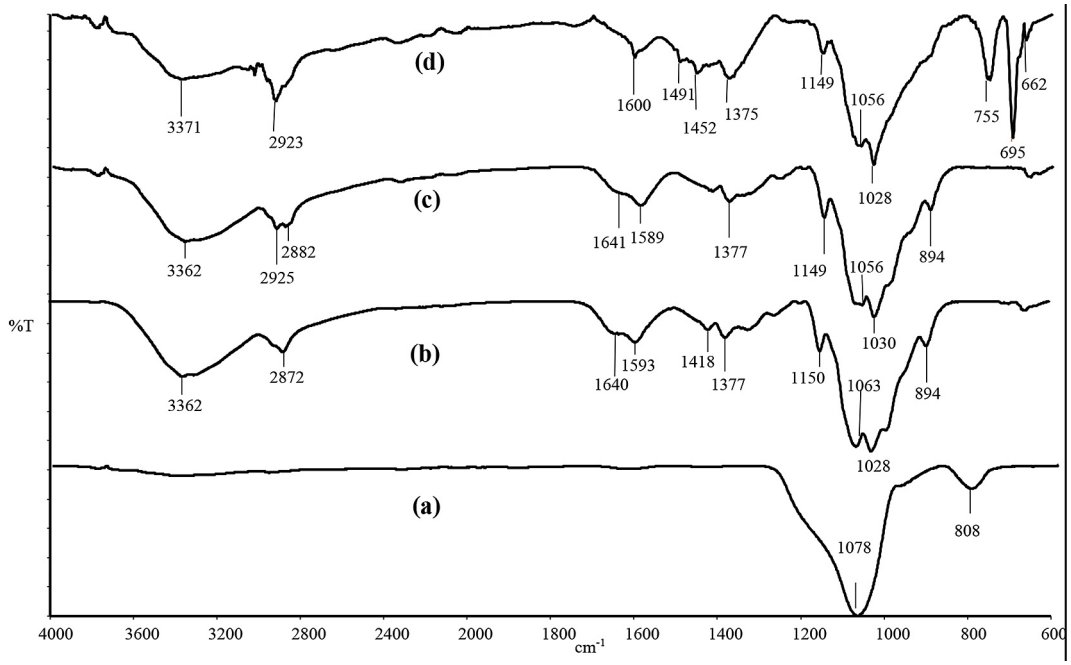

Figure 4. FTIR spectra of (a), FS (b) CS, (c) CS@silica, and (d) REEs-loaded CS@silica

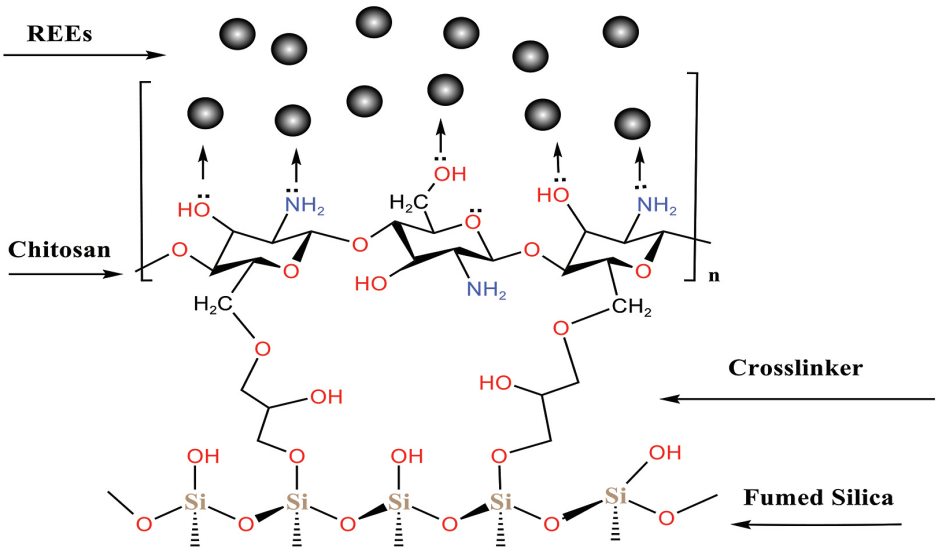

Figure 5. The possible binding mechanism of Ce(III), La(III), and Nd(III) ions on CS@silica composite

CS, FS, CS@silica, and REEs-loaded CS@silica, respectively, using SEM micrographs with a magnification of 1500× along with their EDX spectra. It can be shown that CS has a rough, flaky structure (Figure 6a), whereas FS has a smooth surface (Figure 6b). CS has carbon and oxygen and a small number of nitrogen atoms on its surface, as shown in its EDX peaks (Figure 6a), whereas O and Si atoms are the essential elements in FS, as depicted in Figure 6b. Figure 6c validates the uneven and lumpy surface of CS@silica, typical of composite materials and beneficial for the adsorption process. The CS@silica EDX spectrum, which includes carbon and nitrogen atoms in addition to O and Si

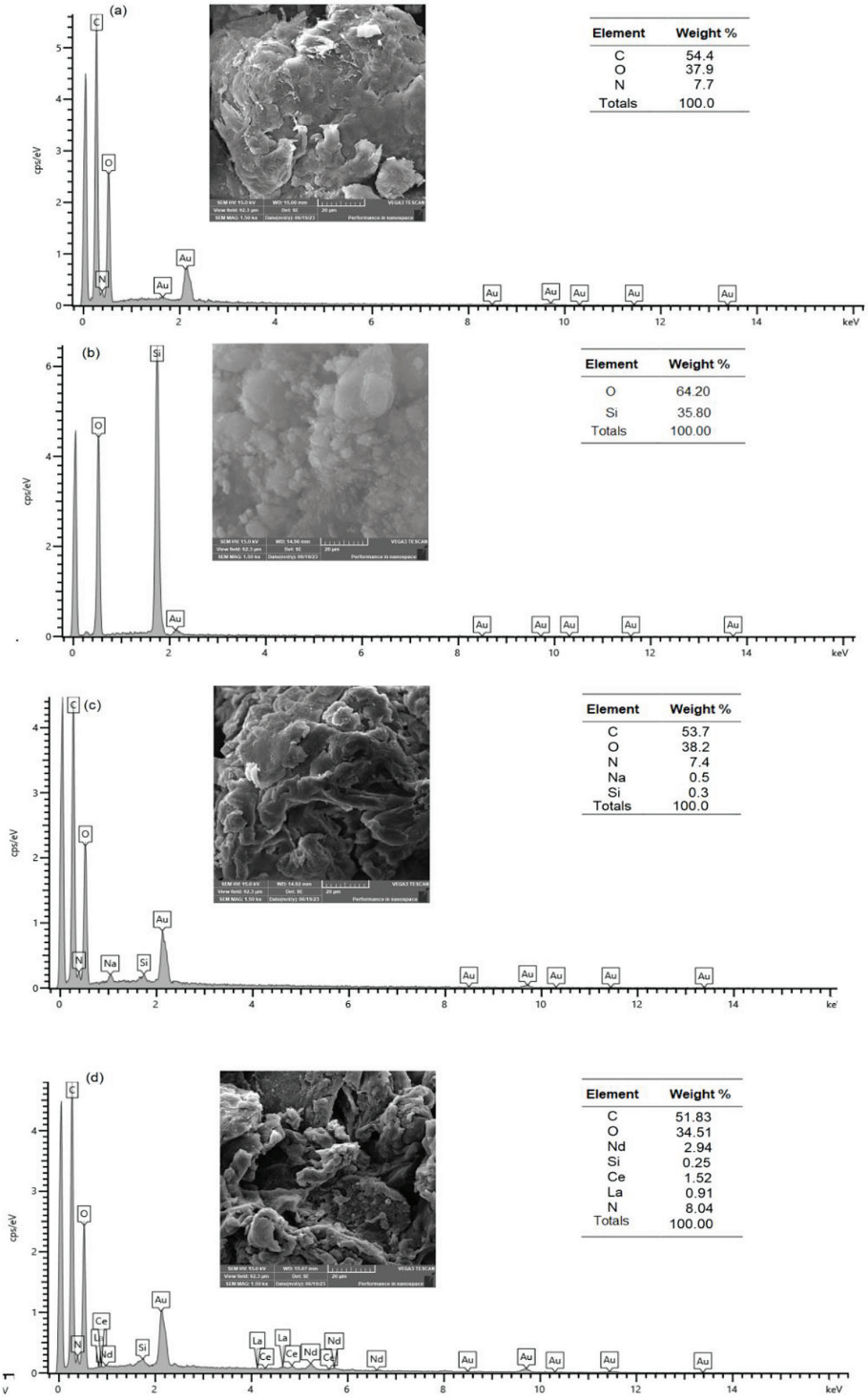

Figure 6. The SEM images and EDX spectra of (a) CS, (b) FS, (c) CS@silica, and (d) REEs-loaded CS@silica, respectively

atoms, further confirms that the CS coating on the FS particles was successful. This is in agreement with the FTIR spectra. A new element of Na atom appeared due to the addition of NaOH solution in the coating process. Following adsorption, the CS@silica surface experienced a reduction in layer size and the emergence of new glossy, voluminous layers attributed to the existence of adsorbed Ce(III), La(III), and Nd(III) cations (Figure 6d). The effective adsorption of these cations by CS@silica composite is confirmed by the EDX image of REEs-loaded CS@silica, which shows similar signals accessible in CS@silica along with the new peaks for the adsorbed REEs on CS@silica composite. The absence of a sodium signal in the spectra of the REEs-loaded CS@silica indicates that sodium ions were released from the composite surface into the solution during the ion exchange process. Furthermore, decreasing the oxygen percentage from 38.32% in CS@silica to 34.51% in REEs-loaded CS@silica suggested that the binding of REEs with O atoms was not the only interaction in the adsorption process, but N atoms may be contributed to the adsorption interaction through a chelation mode as shown in Figure 5.

REEs adsorption tests

Effect of solution pH

The pH value of the liquid may have influenced the metal complexation sites, surface charge, ionization degree, and shape of the metal ions on the adsorbent (Feng et al., 2021). The acidic condition could significantly affect the adsorption of REEs because REE leachates have a high level of acidity (dos Reis et al., 2023b). In low-pH settings, H_3O^+ ions and REEs engage in a competitive process for binding sites, which hinders the adsorption of REEs. In an alkaline medium, REEs undergo precipitation as hydroxides (Javadian et al., 2020). Consequently, this experiment aimed to examine the impact of pH on the adsorption of REEs within the pH range of 2–6. The results of the equilibrium solution pH effect on the CS@silica composite-mediated adsorption of Ce(III), La(III), and Nd(III) cations are displayed in Figure 7. It is noted that the amount adsorbed remained rather consistent, indicating that the principal adsorption process for REEs onto CS@silica is not only based on electrostatic interaction, as it is not significantly affected by changes in pH but chelation or complexation binding is also contributed. The results indicate that the CS@silica composite maintains a stable structure across the pH range tested. In addition, the overlapping of the curves representing the binding of Ce(III) and Nd(III) cations confirms that these two REEs exhibit a highly similar adsorption behavior on the CS@silica composite compared to La(III) cations at various initial solution pH levels (Figure 7). The dissimilarity can be ascribed to the resemblance in ionic radii between Ce(III) and Nd(III) cations,

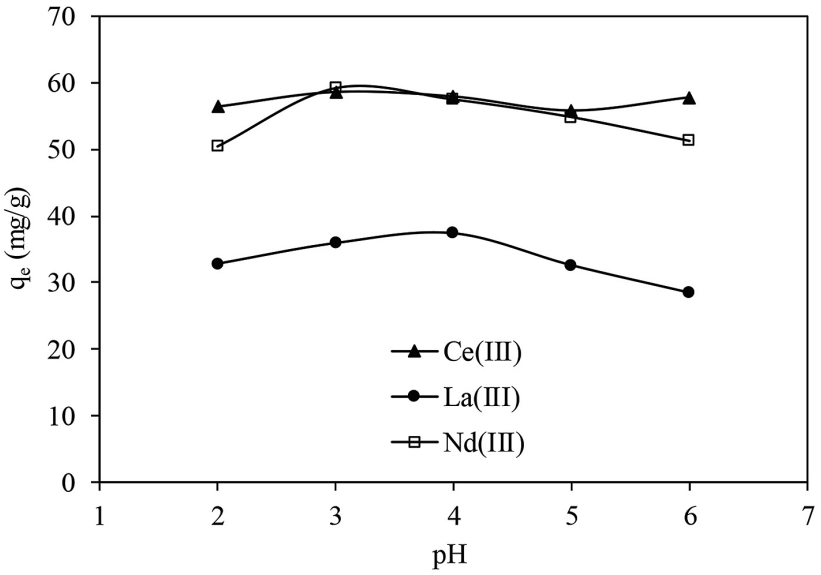

Figure 7. Influence of pH on the adsorbed amount of Ce(III), La(III), and Nd(III) onto CS@silica composite (adsorbent dose of 0.01 g; working volume of 50 mL; REEs concentration of 0.20 mmol/L; and adsorption time of 1 h)

as indicated in Table 2, in contrast to the La(III) cation (Sastri et al., 2003). Predictably, the separation of the three REEs utilizing the CS@silica composite will provide challenges. Moreover, it is worth mentioning that the attraction of Ce(III) and Nd(III) cations to the CS@silica surface was greater compared to La(III) cations, mostly because of the disparities in their electronegativity (Table 2). Due to their elevated electronegativity and compact ionic radius, the Ce(III) and Nd(III) cations will exhibit a stronger attraction towards the oxygen and nitrogen atoms. As a result, the Ce(III) and Nd(III) cations compete with the La(III) cations for the active sites on the CS@silica surface, leading to a decrease in the adsorption affinity of La(III) cations. The literature indicates that the electronegativity of ions influences adsorption. Species with higher electronegativity are more likely to be separated (Sun et al. 2018, dos Reis et al., 2023a). The adsorption capacity for Ce(III) and Nd(III) cations was found to be maximum at pH 3, whereas for La(III) cations, it was highest at pH 4. Additionally, it was observed that when the equilibrium is approached, the pH slightly decreases. Subsequently, additional kinetic and isotherm studies were conducted at a starting pH of 4.

Effect of CS@silica dosage

The quantity of adsorbent used is a crucial aspect that influences the amount of adsorption that can take place. Figure 8(a-c) illustrates the most effective amount of CS@silica required for the adsorption of Ce(III), La(III), and Nd(III) cations. Clearly, increasing the dosage of CS@silica composite from 0.01 to 0.025 g led to higher removal of REEs in the bulk solution, but it also decreased the adsorbed amount of REEs. The enhanced removal can be due to an upsurge in the quantity of energetic sites accessible for the adsorption of REEs. The decrease in the amount of REEs adsorbed may result from the overlapping of adsorption sites or the aggregation of the adsorbent at higher doses. Consequently, the surface area accessible for adsorbate adsorption is reduced (Javadian et al., 2020). Therefore, further examinations on the kinetics and isotherms were carried out utilizing a 0.01 g sample of CS@silica composite.

Adsorption kinetics study

Understanding adsorption kinetics is essential for determining the best parameters for a large-scale batch process. Figure 9(a–d) demonstrates the effect of contact duration on the adsorption of REEs at initial concentrations of 0.20 and 0.40 mmol/L. It is evident that all three REEs showed a consistent trend: there was a rapid increase in adsorption within 5 min, followed by a gradual rise until 60 min, indicating that equilibrium was reached. Furthermore, the amount adsorbed exhibited enhancement when the concentration of REEs increased from 0.20 to 0.40 mmol/L, as evidenced by the data presented in Table 3. This occurs because elevated concentrations of REEs exert a stronger force, allowing them to overcome the barrier to mass transfer between the composite and the liquid (Al-Amrani et al., 2023). Figure 9(a–d) and Table 3 present the obtained fitted kinetic curves and parameters for the adsorption of Ce(III), Nd(III), and La(III) cations onto the CS@silica composite, respectively. Evidently, the PSO kinetic model demonstrates a higher regression coefficient (R^2) and lower χ^2 values compared to the PFO kinetic models. Furthermore, the estimated equilibrium adsorption capacity ($q_{e,cal}$) values derived from the PSO model demonstrate a greater level of similarity to the experimental values, as illustrated in Table 3. Therefore, the PSO model is shown to be the most appropriate for characterizing the dynamic adsorption of Ce(III), Nd(III), and La(III) cations onto the CS@silica composite. It is noteworthy that the adsorption rate of Nd(III) cations was the highest, followed by La(III) and Ce(III) cations, as indicated in Table 3. This aligns with the ionic radii and electronegativity ranking of the examined cations, as listed in Table 2.

Adsorption isotherm study

The adsorption isotherm shape reveals the molecules' adsorption tendency and the stability

Table 2. Properties of the investigated REEs (Yan and Feng, 2009)

Cation	Electron configuration	Ionic radius (Å)	Pauling electronegativity
La(III)	[Xe] $4f^0$	1.032	1.327
Ce(III)	[Xe] $4f^1$	1.010	1.348
Nd(III)	[Xe] $4f^3$	0.983	1.382

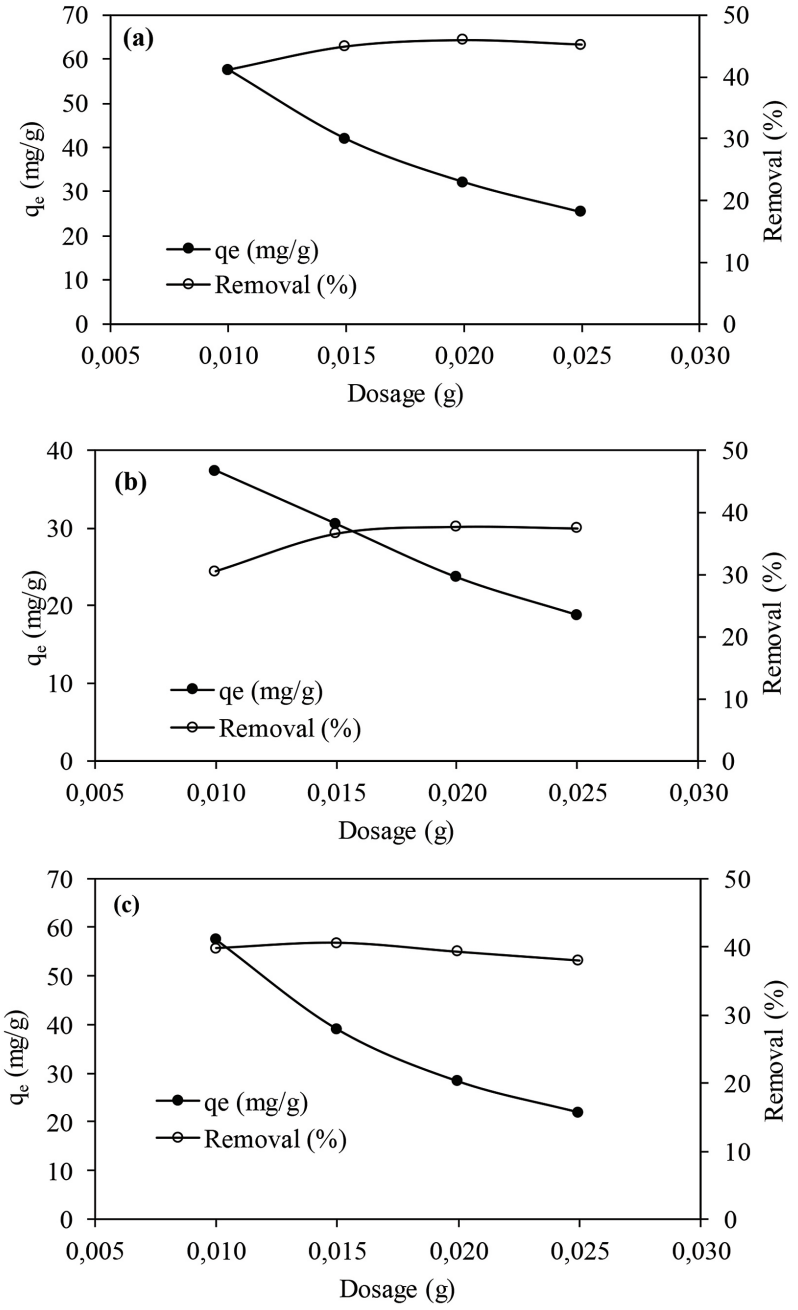

Figure 8. The influence of adsorbent dose on the adsorption of (a) Ce(III), (b) La(III), and (c) Nd(III) on CS@ silica composite (working volume of 50 ml; REEs concentration of 0.20 mmol/L; pH 4 and contact time of 1 h)

of the adsorbate-adsorbent relationship. Adsorption isotherms are also determined by the physicochemical parameters of the adsorbent surface (Sviridova et al., 2022; Mohd Hussin et al., 2024). Figure 10 illustrates the adsorption isotherm of REEs onto CS@silica composite. The adsorption isotherm plot shows an S-shaped isotherm, suggesting that the CS@silica surface has varying energy levels at different adsorption sites. Additionally, REEs do not bind to specific ion exchange sites (Sviridova et al., 2022). The maximal adsorption capacities for Ce(III), La(III), and Nd(III) cations were determined to be 341, 241, and 299 mg/g, respectively.

Comparison of Ce(III), La(III), and Nd(III) on CS@silica composite with other adsorbents found in the literature

The literature provides a compilation of the adsorption capabilities for Ce(III), La(III), and Nd(III) cations on several adsorbents, which can

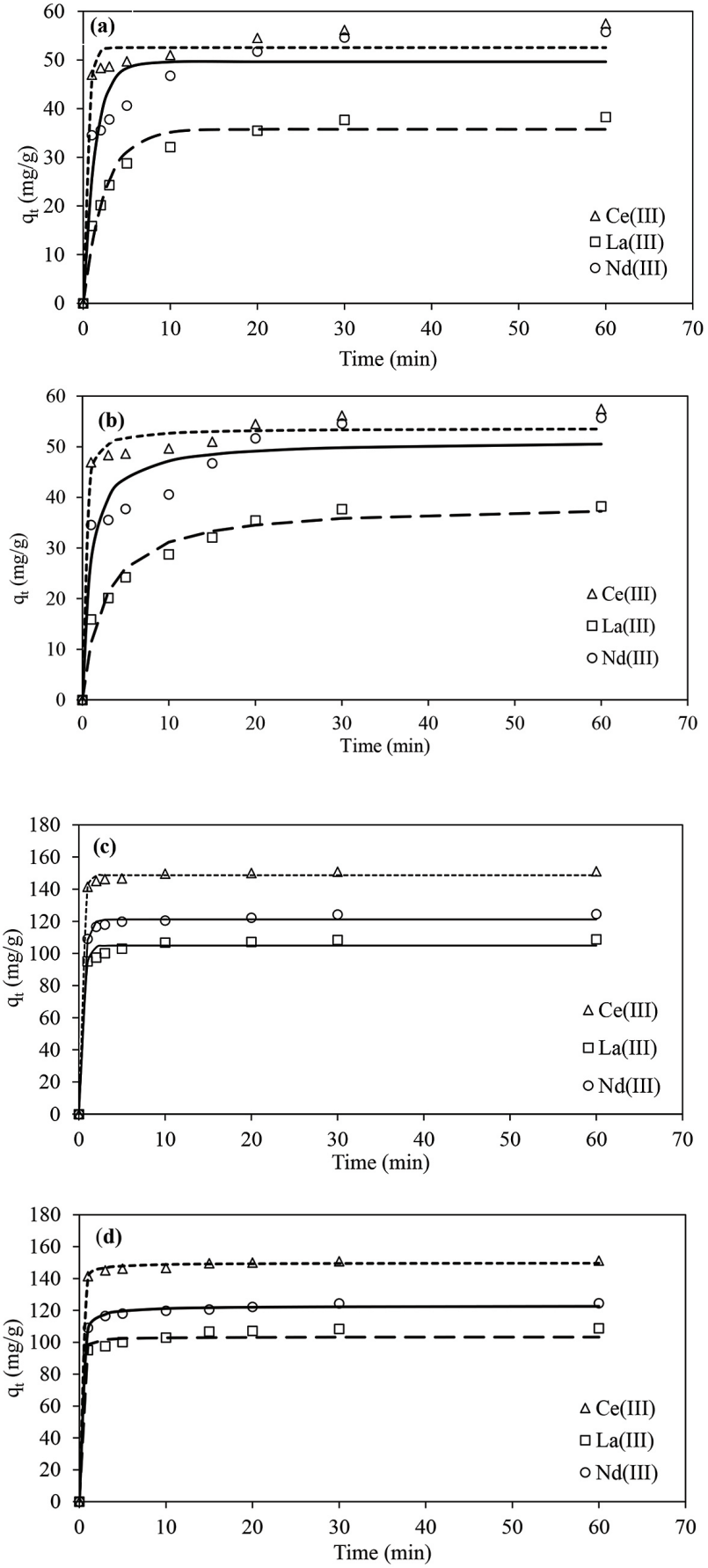

Figure 9. Nonlinear adsorption kinetic plots of (a) PFO, (b) PSO at 0.20 mmol/L, and (c) PFO, (d) PSO at 0.40 mmol/L of Ce(III), La(III) and Nd(III) cations (working volume of 50 mL; and pH 4)

Table 3. Parameters of non-linear PFO and PSO kinetic models adsorption of Ce(III), La(III), and Nd(III) onto CS@silica composite

C_0 (mmol/L)	$q_{e,exp}$ (mg/g)	$q_{e',cal}$ (mg/g)	k_1 (min^{-1})	X^2	R^2	Pseudo-first-order		Pseudo-second-order	
						$q_{e,cal}$ (mg/g)	k_2 (g/mg.min)	X^2	R^2
Ce(III)									
0.20	57.50	52.54	2.07	1.50	0.28	58.14	0.010	1.07	0.49
0.40	151.20	148.63	2.98	0.23	1.00	149.78	0.010	0.10	0.81
La(III)									
0.20	38.25	35.74	0.41	2.49	0.91	38.77	0.01	2.07	0.92
0.40	108.80	104.90	2.22	0.98	0.48	106.62	0.06	0.51	1.00
Nd(III)									
0.20	55.75	49.63	0.73	6.89	0.51	51.24	0.02	5.17	0.92
0.40	124.55	121.16	2.24	0.38	0.75	122.82	0.06	0.13	0.99

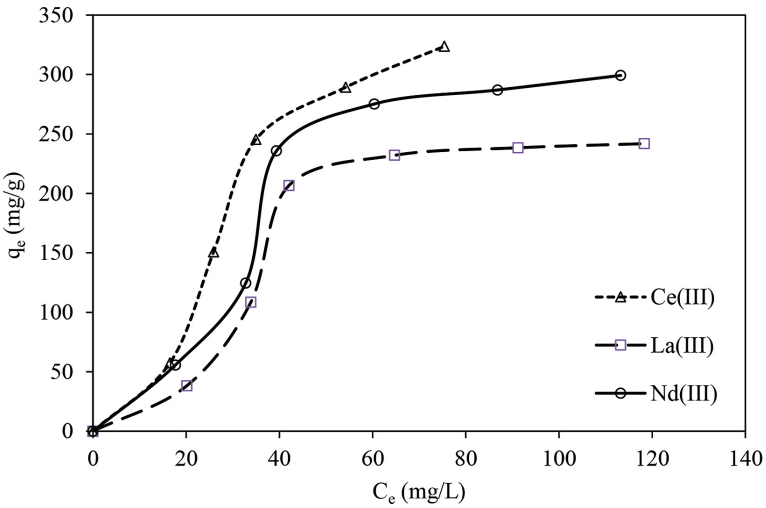

Figure 10. Isotherm plots for the adsorption of Ce(III), La(III), and Nd(III) on CS@ silica composite (working volume of 50 ml; contact time of 60 min; adsorbent dose of 0.01 g; REEs concentration in the range of 0.20 to 1.20 mmol/L; and pH 4)

be found in Table 4. Table 4 shows that the CS@ silica composite had a highly competitive and effective retrieval for the three REEs. The CS@ silica material shows rapid adsorption of three REEs from the liquid phase simultaneously within 5 min. Nevertheless, the adsorbent $MnFe_2O_4$@ SiO_2-CS (Liu et al., 2021) exhibited significantly higher q_{max} values for La(III) and Ce(III) cations. However, the preparation process for this adsorbent is considerably more complicated.

Desorption study

An investigation into the desorption of REEs from the used adsorbent is necessary in order to separate and retrieve REEs. Therefore, the CS@ silica composite containing three REEs was tested for desorption in neutral and acidic solutions, including deionized water and two concentrations of HCl (0.01 and 0.02 mol/L). The results of the desorption process are presented in Table 5. The desorption percentages are consistently low for all the eluents under investigation. The recovery rate ranges from 2.6 to 3.28%, potentially attributed to the occurrence of an ion-exchange interaction. The relationship between REEs and CS@silica composite likely extended beyond electrostatic forces and encompassed additional robust chemical interactions, such as electron sharing and covalent interactions (Lakić et al., 2023). Therefore, the desorption investigation yielded results that were in line with the findings from the previous experiments on pH solution and kinetics.

Table 4. Comparison of CS@silica adsorption capacity for Ce(III), La(III), and Nd(III) cations with other reported adsorbents

Adsorbent	Optimum experimental adsorption conditions					Adsorption capacity (mg/g)			References
	Initial REEs conc. (mg/L)	Equilibrium time (min)	pH	Temp. (°C)	Adsorbent dose (g/L)	La(III)	Ce(III)	Nd(III)	
Chitosan-coated fumed silica (CS@silica)	0–144	20	4.0	30	0.2	241	341	299	This study
Diatomite	0–100	120	2.0	25	1.0	23	56	101	(dos Reis et al., 2023a)
Chitosan powder	0–300	150	6.0	25	1.0	85	-	-	(dos Reis et al., 2022)
Chitosan film						94	-	-	
Chitosan spongy						266	-	-	
EDTA–CS@ZIF-8	0–200	1440	6.0	25	1.5×10^{-3}	256	-	-	(Feng et al., 2021)
Magnetic-chitosan-urea (MC-UR)	1–500	60	5.0	25	0.4	-	119	-	(Hamza et al., 2022)
Magnetic calcium alginate/ carboxymethyl chitosan/ $Ni_{0.2}Zn_{0.2}Fe_{2.6}O_4$ (CA/CMC/ $Ni_{0.2}Zn_{0.2}Fe_{2.6}O_{4)}$	30	63	5.5	25	0.8	-	-	23	(Javadian et al., 2020)
Chitosan acryloylthiourea CATU	50–1000	240	5.0	25	1.0	291	-	-	(Khalil et al., 2018)
AEAM-PTMS@silica	72–1442	360	7.5	25	0.02	-	-	68	(Lakić et al., 2023)
$MnFe_2O_4$@SiO_2-CS	10–500	120	7.0	25	0.3	1030	1020	-	(Liu et al., 2021)
EDTA-chitosan–silica	-	60	3.0	25	2.5	-	-	61	(Roosen et al., 2014)
DTPA-chitosan–silica			4.0			-	-	107	
DT-GMA-MBA/SiO_2	89–510	30-40	4.0	22	1.25	-	-	130	(Salih et al., 2021)
PEI-chitosan	5–500	120	3.5	25	1.0	280	-	-	(Zhao et al., 2020)
Carboxylated graphene oxide/diatomite/magnetic chitosan (GOH/DMCS)	50	50	8.0	35	3.0	303	-	-	(Zhou et al., 2021)

Table 5. Desorption of the analyzed REEs from the spent CS@silica composite

Eluent	Desorption (%)		
	Ce(III)	La(III)	Nd(III)
Deionized water	0.32	0.34	0.27
0.01 M HCl	2.23	2.36	1.92
0.02 M HCl	3.09	3.28	2.60

CONCLUSIONS

The work successfully synthesized a CS@silica composite and utilized it to simultaneously recover three REEs (Ce(III), La(III), and Nd(III)) from a water-based solution. The characterization outcomes from elemental analysis, EDX, and FTIR spectra indicate that the CS@silica surface contains a significant number of nitrogen (N) and oxygen (O) atoms. The best conditions for adsorbing REEs utilizing CS@silica composite are a dosage of 0.01 g, a pH of 4, and a contact period of 20 min. The findings indicate that the REE adsorption was not significantly influenced by the solution pH. The adsorption process follows the pseudo-second-order kinetic model, reaching equilibrium in 20 min, indicating a rapid REE adsorption with the CS@silica composite. The S-shaped isotherm illustrates the variation in energy levels of functional groups on the composite

surface. The desorption investigation provides evidence of the high affinity of the REEs for the binding sites on the CS@silica composite surface. Complexation is one of the dominant mechanisms responsible for the adsorption of Ce(III), La(III), and Nd(III). The CS@silica composite, with its exceptional properties, simple synthesis technique, and rapid kinetics, is considered one of the most promising adsorbents for the recovery of REEs.

Acknowledgement

The authors are grateful to the funds provided by Kurita Water and Environment Foundation (KWEF, Grant number: 22Pmy009-A6 (100-TNCPI/INT 16/6/2 (077/2022)), Japan.

REFERENCES

1. Ahmed, M.J., Hameed, B.H. and Hummadi, E.H. 2020. Review on recent progress in chitosan/chitin-carbonaceous material composites for the adsorption of water pollutants. Carbohydrate Polymers, 247, 116690. https://doi.org/10.1016/j.carbpol.2020.116690
2. Al-Amrani, W.A., Abdullah, R., Megat Hanafiah, M.A.K. and Mohd Suah, F.B. 2023. Removal of Ni(II) Ions by citric acid-functionalized *Aloe vera* Leaf Powder – Characterisation, Kinetics, and Isotherm Studies. Journal of Ecological Engineering, 24(4), 217–227. 10.12911/22998993/159633
3. Al-Amrani, W.A., Hanafiah, M.A.K.M. and Mohammed, A.H.A. 2022. A comprehensive review of anionic azo dyes adsorption on surface-functionalised silicas. Environmental Science and Pollution Research https://doi.org/10.1007/s11356-022-23062-0
4. Arciszewska, Ż., Gama, S., Leśniewska, B., Malejko, J., Nalewajko-Sieliwoniuk, E., Zambrzycka-Szelewa, E. and Godlewska-Żyłkiewicz, B. 2022. The translocation pathways of rare earth elements from the environment to the food chain and their impact on human health. Process Safety and Environmental Protection, 168, 205–223. https://doi.org/10.1016/j.psep.2022.09.056
5. Asadollahzadeh, M., Torkaman, R. and Torab-Mostaedi, M. 2021. Extraction and separation of rare earth elements by adsorption approaches: current status and future trends. Separation & Purification Reviews, 50(4), 417–444. 10.1080/15422119.2020.1792930.
6. Atia, A.A., Doni, A.M. and Al-Amrani, W.A. 2009. Adsorption/desorption behavior of acid orange 10 on magnetic silica modified with amine groups. Chemical Engineering Journal, 150, 55–62. http://doi.10.1016/j.cej.2008.12.004
7. Benettayeb, A., Seihoub, F.Z., Pal, P., Ghosh, S., Usman, M., Chia, C.H., Usman, M. and Sillanpää, M. 2023. Chitosan nanoparticles as potential nanosorbent for removal of toxic environmental pollutants. Nanomaterials, 13(3), 447.
8. Budnyak, T.M., Błachnio, M., Slabon, A., Jaworski, A., Tertykh, V.A., Deryło-Marczewska, A. and Marczewski, A. W. 2020. Chitosan deposited onto fumed silica surface as sustainable hybrid biosorbent for acid orange 8 dye capture: Effect of temperature in adsorption equilibrium and kinetics. The Journal of Physical Chemistry C, 124(28), 15312–15323. 10.1021/acs.jpcc.0c04205
9. Donia, A.M., Atia, A.A., Al-amrani, W.A. and M., E.-N.A. 2009. Effect of structural properties of acid dyes on their adsorption behaviour from aqueous solutions by amine modified silica. Journal of Hazardous Materials, 161, 1544–1550. http://10.1016/j.jhazmat.2008.05.042
10. dos Reis, G.S., Dotto, G.L., Vieillard, J., Oliveira, M.L.S., Lütke, S.F., Silva, L.F.O., Lima, É.C., Salau, N.P.G. and Lassi, U. 2023a. Uptake the rare earth elements Nd, Ce, and La by a commercial diatomite: kinetics, equilibrium, thermodynamic and adsorption mechanism. Journal of Molecular Liquids, 389, 122862. https://doi.org/10.1016/j.molliq.2023.122862
11. dos Reis, G.S., Pinto, D., Lima, É.C., Knani, S., Grimm, A., Silva, L.F.O., Cadaval, T.R.S. and Dotto, G.L. 2022. Lanthanum uptake from water using chitosan with different configurations. Reactive and Functional Polymers, 180, 105395. https://doi.org/10.1016/j.reactfunctpolym.2022.105395
12. dos Reis, G.S., Pinto, D., Lütke, S.F., Lima, É., Silva, L.F.O., De Brum, I.A.S. and Dotto, G.L. 2023b. Adsorption of yttrium (Y^{3+}) and concentration of rare earth elements from phosphogypsum using chitin and chitin aerogel. Journal of Rare Earths. https://doi.org/10.1016/j.jre.2023.04.008
13. Feng, S., Du, X., Bat-Amgalan, M.; Zhang, H., Miyamoto, N. and Kano, N. 2021. Adsorption of REEs from aqueous solution by EDTA-chitosan modified with zeolite imidazole framework (ZIF-8). International Journal of Molecular Sciences, 22, 344. https://doi.org/10.3390/ijms22073447
14. Hamza, M.F., Guibal, E., Abdel-Rahman, A.A.-H., Salem, M., Khalafalla, M.S. and Wei, Y.Y.X. 2022. Enhancement of Cerium sorption onto Urea-Functionalized magnetite chitosan microparticles by sorbent sulfonation – Application to ore leachate. Molecules 27, 7562. https://doi.org/10.3390/molecules27217562
15. Ho, Y.S. and McKay, G. 1999. Pseudo-second order model for sorption processes. Process Biochemistry, 34(5), 451–465. https://doi.org/10.1016/S0032-9592(98)00112-5
16. Iftekhar, S., Heidari, G., Amanat, N., Zare, E.N., Asif, M.B., Hassanpour, M., Lehto, V.P. and

Sillanpaa, M. 2022. Porous materials for the recovery of rare earth elements, platinum group metals, and other valuable metals: A review. Environmental Chemistry Letters, 20(6), 3697–3746.

17. Javadian, H., Ruiz, M. and Sastre, A.M. 2020. Response surface methodology based on central composite design for simultaneous adsorption of rare earth elements using nanoporous calcium alginate/carboxymethyl chitosan microbiocomposite powder containing Ni0.2Zn0.2Fe2.6O4 magnetic nanoparticles: Batch and column studies. International Journal of Biological Macromolecules, 154, 937–953. https://doi.org/10.1016/j.ijbiomac.2020.03.131
18. Jemli, S., Pinto, D., Kanhounnon, W. G., Ben Amara, F., Sellaoui, L., Bonilla-Petriciolet, A., Dhaouadi, F., Ameri, R., Silva, L.F.O., Bejar, S., Dotto, G.L. and Badawi, M. 2023. Green β-cyclodextrin nanosponges for the efficient adsorption of light rare earth elements: Cerium and lanthanum. Chemical Engineering Journal, 466, 143108. https://doi.org/10.1016/j.cej.2023.143108
19. Khalil, M.M.H., Atrees, M.S., Abd El Fatah, A.I. L., Salem, H. and Roshdi, R. 2018. Synthesis and application studies of chitosan acryloylthiourea derivative for the separation of rare earth elements. Journal of Dispersion Science and Technology, 39(4), 605-613. 10.1080/01932691.2017.1370674
20. Lagergren, S.K. 1898. About the theory of so-called adsorption of soluble substances. Sven Vetenskapsakad Handingar, 24, 1–39.
21. Lakić, M., Breijaert, T.C., Daniel, G., Svensson, F. G., Kessler, V.G. and Seisenbaeva, G.A. 2023. Uptake and separation of rare earth elements and late transition metal cations by nanoadsorbent grafted with diamino ligands. Separation and Purification Technology, 323, 124487. https://doi.org/10.1016/j.seppur.2023.124487.
22. Liu, Z., Chen, G., Li, X. and Lu, X. 2021. Removal of rare earth elements by $MnFe_2O_4$ based mesoporous adsorbents: Synthesis, isotherms, kinetics, thermodynamics. Journal of Alloys and Compounds, 856, 158185. https://doi.org/10.1016/j.jallcom.2020.158185.
23. Martinez-Gomez, N.C., Vu, H.N. and Skovran, E. 2016. Lanthanide chemistry: From coordination in chemical complexes shaping our technology to coordination in enzymes shaping bacterial metabolism. Inorganic Chemistry, 55(20), 10083–10089. 10.1021/acs.inorgchem.6b00919
24. Mohd Hussin, S., Al-Amrani, W.A., Mohd Suah, F.B., Harimu, L. and Hanafiah, M.A.K.M. 2024. Hydrogen peroxide treated desiccated coconut waste as a biosorbent in malachite green removal from aqueous solutions. Journal of Ecological Engineering, 25(3), 323–333. https://doi.org/10.12911/22998993/182870
25. Ponou, J., Wang, L.P., Dodbiba, G., Okaya, K., Fujita, T., Mitsuhashi, K., Atarashi, T., Satoh, G. and Noda, M. 2014. Recovery of rare earth elements from aqueous solution obtained from Vietnamese clay minerals using dried and carbonized parachlorella. Journal of Environmental Chemical Engineering, 2(2), 1070–1081. https://doi.org/10.1016/j.jece.2014.04.002
26. Qiu, Y., Ding, K., Tang, L., Qin, Z., Li, M. and Yin, X. 2022. Water-recyclable chitosan-based ion-imprinted thermoresponsive hydrogel for rare earth metal ions accumulation. International Journal of Molecular Sciences, 23(18), 10542.
27. Rahman, M.M., Awual, M.R. and Asiri, A.M. 2020. Preparation and evaluation of composite hybrid nanomaterials for rare-earth elements separation and recovery. Separation and Purification Technology, 253, 117515. https://doi.org/10.1016/j.seppur.2020.117515
28. Roosen, J., Spooren, J. and Binnemans, K. 2014. Adsorption performance of functionalized chitosan–silica hybrid materials toward rare earths. Journal of Materials Chemistry A, 2, 19415. http://doi:10.1039/c4ta04518a
29. Ryu, S., Fonseka, C., Naidu, G., Loganathan, P., Moon, H., Kandasamy, J. and Vigneswaran, S. 2021. Recovery of rare earth elements (Lu, Y) by adsorption using functionalized SBA-15 and MIL-101 (Cr). Chemosphere, 281, 130869. https://doi.org/10.1016/j.chemosphere.2021.130869
30. Salih, K.A.M., Hamza, M.F., Mira, H., Wei, Y., Gao, F., Atta, A.M., Fujita, T. and Guibal, E. 2021. Nd(III) and Gd(III) sorption on mesoporous amine-functionalized polymer/SiO_2 composite. Molecules, 26(4), 1049.
31. Sastri, V.R., Perumareddi, J.R., Rao, V.R., Rayudu, G.V.S. and Bünzli, J.C. 2003. Modern aspects of rare earths and their complexes, Elsevier.
32. Sun, Z., Chai, L., Liu, M., Shu, Y., Li, Q., Wang, Y. and Qiu, D. 2018. Effect of the electronegativity on the electrosorption selectivity of anions during capacitive deionization. Chemosphere, 195, 282–290.
33. Sviridova, A.V., Maltseva, G.I. and Timofeev, K.L. 2022. Adsorption of metalions on aluminosilicates. Russian Journal of Physical Chemistry A, 96(12), 2737–2746. http://doi.10.1134/S0036024422120263
34. Yan, L.K. and Feng, X.D. 2009. New development of concept of electronegativity Chinese Science Bulletin, 54(2), 328–334.
35. Zhao, F., Yang, Z., Wei, Z., Spinney, R., Sillanpää, M., Tang, J., Tam, M. and Xiao, R. 2020. Polyethylenimine-modified chitosan materials for the recovery of La(III) from leachates of bauxite residue. Chemical Engineering Journal, 388, 124307. https://doi.org/10.1016/j.cej.2020.124307
36. Zhou, J., Song, X., Shui, B. and Wang, S. 2021. Preparation of graphene oxide composites and assessment of their adsorption properties for Lanthanum (III). Coatings, 11, 1040. https://doi.org/10.3390/oatings11091040